Exploring the Ub/UBL landscape with activity-based probes

Witting, K.F.

Chapter 6

RPL26-UFMylation promotes interaction with SRP receptor during protein translocation

Katharina F. Witting, Zhenyu Xiao, Roman Gonzalez-Pietro, Birol Cabukusta, Fabricio Loayza-Puch, Alfred C.O. Vertegaal, Reuven Agami, Jacques Neefjes, Huib Ovaa

Abstract

UFM1, a Ubiquitin-like reversible posttranslational modification (PTM), is covalently attached to the lysine residues of its substrate proteins through the orchestrated action of its specialized conjugation enzymes and detached by a dedicated protease—UFSP2. Despite a rudimentary biochemical and structural understanding the enzymatic cascade, the biological role of UFM1 remains enigmatic due to the lack of knowledge of its substrates. To address this unmet need, we devised a proteomics strategy to uncover UFMylated substrates, permitting a deeper understanding of the cellular function of UFM1. One of the predominant UFSP2-dependent substrates—the ribosomal protein RPL26—acquires affinity for the signal recognition particle receptor alpha (SRα) upon UFMylation. Moreover, we observed that translational arrest induces UFMylation of the ribosome, which may provide a means to pause polypeptide elongation and subsequently recruit the signal recognition particle receptor α subunit (SRα). Collectively, our data indicate that ribosomal UFMylation in conjunction with perturbed ribosomal translation dynamics modulates SRP-dependent ER-targeting.

Introduction

Post-translational modification of proteins with the Ubiquitin-like modifier UFM1, affects a wide variety of cellular process ranging from hematopoiesis, translation, ER homeostasis, as well as ribosomal function[1-9]. While aberrations of the ligating and deconjugating enzymes have been associated with a variety of human diseases such as cancer, diabetes, schizophrenia, and cardiovascular diseases, genetic loss of function mutations primarily affect brain, erythroid, and liver development during embryonic development, the direct contribution of UFM1 to the pathogenesis of these diseases needs to be established[6, 10-18]. Covalent attachment of UFM1 to the lysine residues of its substrate proteins is initiated through the adenylation of the C-terminal glycine of UFM1 by UBA5 (E1) and subsequent nucleophilic attack by the active site cysteine. Concurrently, activated UFM1 is relayed to UFC1 (E2) through trans-thioesterification, rekindling thioester formation and mediating its transfer to the lysine residues of its substrates with the assistance of the E3-like enzyme UFL1[19]. Eventual detachment is accomplished by its dedicated cysteine protease UFSP2[20], conferring this PTM its dynamic nature. Additionally, self-modification of UFM1 yields the formation of a K69-linked poly-UFM1 chain[10], evoking recruitment of adaptor proteins.

While the structural and the biochemical features of some of the UFM1 conjugating and deconjugating enzymes are gradually being unraveled, the physiological role of UFMylation remains enigmatic primarily due to lack of knowledge of its substrates. Yet, in contrast to Ubiquitination and SUMOylation, where techniques such as diGly proteomics and affinity-capture methods[21] have propelled the discovery of their substrates, analogous approaches are virtually nonexistent for UFM1. Given the lack of appropriate tools and the low abundance of UFM1, identification of only a few substrates has been accomplished, primarily by affinity capture using overexpressed epitope-tagged UFM1[22]. The few proteins identified as UFM1 substrates include the estrogen receptor alpha (ERα) activating signal co-integrator ASC1, the UFM1 interacting protein DDRGK (or UFBP1), the ribosomal proteins RPS3 (uS3), RPS20 (uS10), RPL10 (uL16) as well as the cytochrome reductase CYB5R3 and the proteasomal subunit PSMB5[22]. However, the cellular function as well as the underlying molecular mechanisms of UFMylation still remain obscure thus necessitating the development of a suitable proteomics strategy.

To achieve this, we adapted the proteomic method originally employed for site-specific mapping of the SUMO proteome[23] in combination with CRISPR-Cas mediated depletion of UFSP2 to enhance UFMylation. This approach allowed the identification of several UFM1 modified proteins involved in DNA replication, vesicle trafficking, and protein translation, with the ribosomal protein RPL26 (uL24) and its paralog RPL26L1 being the most prominent target. In order to dissect the physiological role of RPL26-UFMylation, we hypothesized that this post-translational modification might evoke the recruitment of specific ribosome

interactors. In agreement with the recent report by Walczak *et al.*[7], we found that RPL26 UFMylation promotes ribosomal membrane association. Moreover, we discovered that UFMylated ribosomes promote the direct interaction of the ribosome with SRα, implying the participation of UFM1 in SRP pathway. More strikingly, we demonstrate that perturbation of ribosomal function with translational inhibitors such as cycloheximide and anisomycin induced RPL26-UFMylation, strongly suggesting that UFM1 impinges translational activity perhaps coupling translation and translocation. Collectively, these discoveries indicate that ribosomal UFMylation not only partakes in co-translational protein translocation through interaction with SRα, but also seems to be involved in the translational cycle in general.

Results

UFSP2 depletion enriches UFMylated substrates

To chart the UFM1 proteome, we adapted the proteomics strategy reported by Hendricks *et al*., for mapping SUMO conjugation sites by generating HeLa cells stably expressing His10-UFM1(K0) in which all lysines were replaced by arginine to prevent poly-UFM1 chain formation[23] (Figure 1B). Given the low abundance of UFMylation, we enriched for UFMylated proteins through CRISPR-Cas9 mediated depletion of the only known UFM-1 specific protease—UFSP2—revealing two prominent targets (Figure 1A). Pulldown of His10-UFM1-modified proteins under denaturing conditions in UFSP2 depleted cells led to the accumulation primarily of singly and doubly modified RPL26 and its paralog RPL26L1 (Figure 1C and S1C). Interestingly, the appearance of unique bands in these cells suggest that other proteins including the DNA replication licensing factor MDM5, WD-repeat protein WDR63, the anion exchange transporter SLC26A7, and the pseudokinase SCYL2 are also regulated by UFMylation in a UFSP2-dependent manner (Figure 1C and Figure S1A and S1C). Since this proteomics method allows the precise identification of the acceptor lysines, we could pinpoint the modification sites of seven identified substrates (Figure S1C). Given that both UFM1 and RPL26/RPL26L1 are highly conserved throughout a variety of species, we decided to explore the molecular function of UFMylated-RPL26 especially in the context of translation. Similar to Walczack *et al.*[7], we observe UFM-1 conjugation preferentially at the C-terminal acceptor lysines K132 and K134 of RPL26/RPL26L1, however, we also detect two additional acceptor lysines (K136 and K142) which are utilized albeit less efficiently (Figure S1B and S1C).

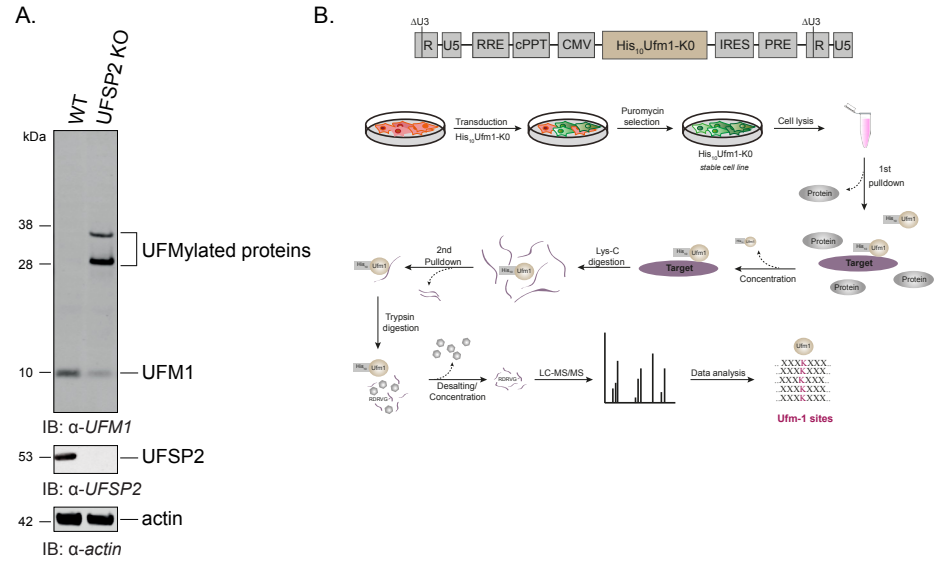

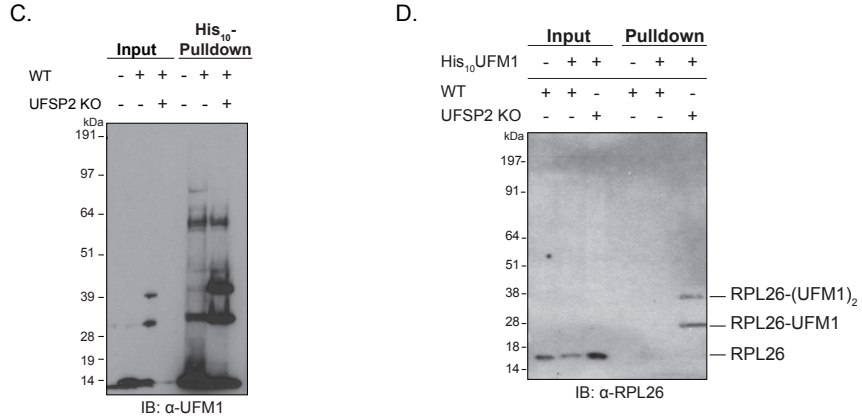

Figure 1| Identification of UFMylated substrates by mass spectrometry. A) Depletion of UFSP2 leads to accumulation of two prominent UFMylated target proteins as assessed by immunoblotting. B) Scheme depicting the strategy for enriching UFMylated substrates and the corresponding acceptor lysines using a method adapted from Hendriks *et al.*[23]. C) Pulldown of UFM1 conjugates from HeLa cells stably expressing His10-UFM1 in the presence or absence of UFSP2 and subsequent immunoblotting with the indicated antibodies. D) Samples were analyzed as in C) by immunoblotting against RPL26 to confirm that endogenous RPL26 is UFMylated, as identified by mass spectrometry.

UFMylated ribosomes promote interaction with the signal recognition particle receptor

It is well established that the ribosome is post-translationally modified for example by phosphorylation, Ubiquitination, or more recently UFMylation[7, 8, 24] primarily to modulate translation in response to cellular stressors[25-27] or to attract specific interacting proteins to potentially modulate its activity[24]. Given the proximity of RPL26 to the crowded ribosomal tunnel exit, its C-terminal UFMylation creates a surface-exposed extension (Figure 2A), which we hypothesize could potentially determine the ribosome's interactome during specific translational phases or during SRP-dependent protein translocation.

To verify our hypothesis that UFMylation could possibly alter the ''ribo-interactome'', we transiently over-expressed RPL26-FLAG in both wild type and UFSP2-depleted HeLa cells and co-immunoprecipitated the containing ribosomes prior to mass spectrometric analysis. This approach permitted us to discriminate between two scenarios: Firstly, ribosomes with dynamic UFMylation and Secondly, constitutively UFMylated ribosomes (Figure 2B). Intriguingly, we found that the cytosolic alpha subunit of the signal recognition particle (SRα) contacts ribosomes UFMylated at RPL26. Further validation by co-immunoprecipitation of endogenous UFMylated RPL26 or by SRα confirms that the affinity of these components is UFM1-dependent (Figure 2C and D). Similarly, ectopically expressed FLAG-SRα interacts only with UFM1-modified RPL26, underscoring that this post-translational modification of the ribosome confers its increased affinity for the SRα receptor (Figure 2C-E). In line with previous observations[7], differential centrifugation of UFSP2-depleted HeLa cell lysates followed by ribosome pelleting over a sucrose cushion established that UFM-1 modified ribosomes associate with ER membranes, implying that UFMylation also governs ribosome localization[7] (Figures S2B and 2C).

Signal recognition particle (SRP)-dependent protein translocation, which permits protein targeting of membrane and cytosolic proteins to the ER[28-30], depends on the initial recognition of the nascent hydrophobic signal peptide emerging from the ribosome by the SRP[31-33]. Upon binding of SRP to the emerging signal sequence and simultaneous structural reorganization of SRP54, the SRP- ribosome nascent chain complex (RNC) complex is recruited to the ER-membrane bound signal recognition particle receptor (SRβ) homodimer in a GTP-dependent manner forming the primary constituents of the targeting complex (TC). Subsequent to SR engagement with the SRP-RNC complex, the nascent peptide is transferred to the translocon, instigating displacement of the TC under GTP hydrolysis thereby priming another targeting cycle[31].

The SRα consists of three domains—a SRβ-interacting SRX domain, a ribosome binding region (RBR) domain, and the N-terminal GTPase (NG)-domain[31, 34]. While the SRX domain interacts with SRβ in a GTP-dependent manner and is dispensable for the catalytic activity of SRα[31, 34], the C-terminal NG-domain of SRα is indispensable to facilitate the GTP-dependent dimerization of SRα and SRP54[35]. Embedded between these two domains is the linker region harboring the RBR domain[31, 34].

To dissect which domain of SRα mediates the binding of the UFMylated ribosome, we co-immunoprecipitated ribosomes with or without UFMylation with truncated versions of SRα containing an intact NG-domain to allow dimerization with SRP54 and thereby preserving its functionality. Interestingly, a marked affinity of the ribosome binding region (RBR) of the SRα with UFMylated ribosomes comparable with that of the untruncated SRα is observed (Figure 2F). Although this domain has previously been reported to directly bind to ribosomes *in vitro*[34, 36], we demonstrate that this domain strongly associates with UFMylated RPL26 *in vivo* (Figure 2F). While earlier in vitro studies have implied that SRα is crucial for transfer of the signal peptide from the ribosome-nascent-chain (RNC) complex to the SEC61 translocon [37, 38] most likely with participation of its ribosomal binding site, we provide evidence that the direct ribosome-SRα interaction in mammalian cells occurs in a UFM1-dependent manner (Figure 2C-F).

To accommodate interaction of SRα with the ribosome in the presence of signal recognition particle, translation is temporarily halted to coordinate the required structural changes before insertion of a peptide into the SEC61 translocon[39]. This observation, however, contradicts the reported direct interaction between UFMylated RPL26 and the translocon (SEC61 and SEC62[7] as well as our own experiments in which we could not recapitulate the reported interaction. An association of the translocon with the UFMylated ribosome would require actively translating ribosomes, which would preclude the binding to the SRP and SRα.

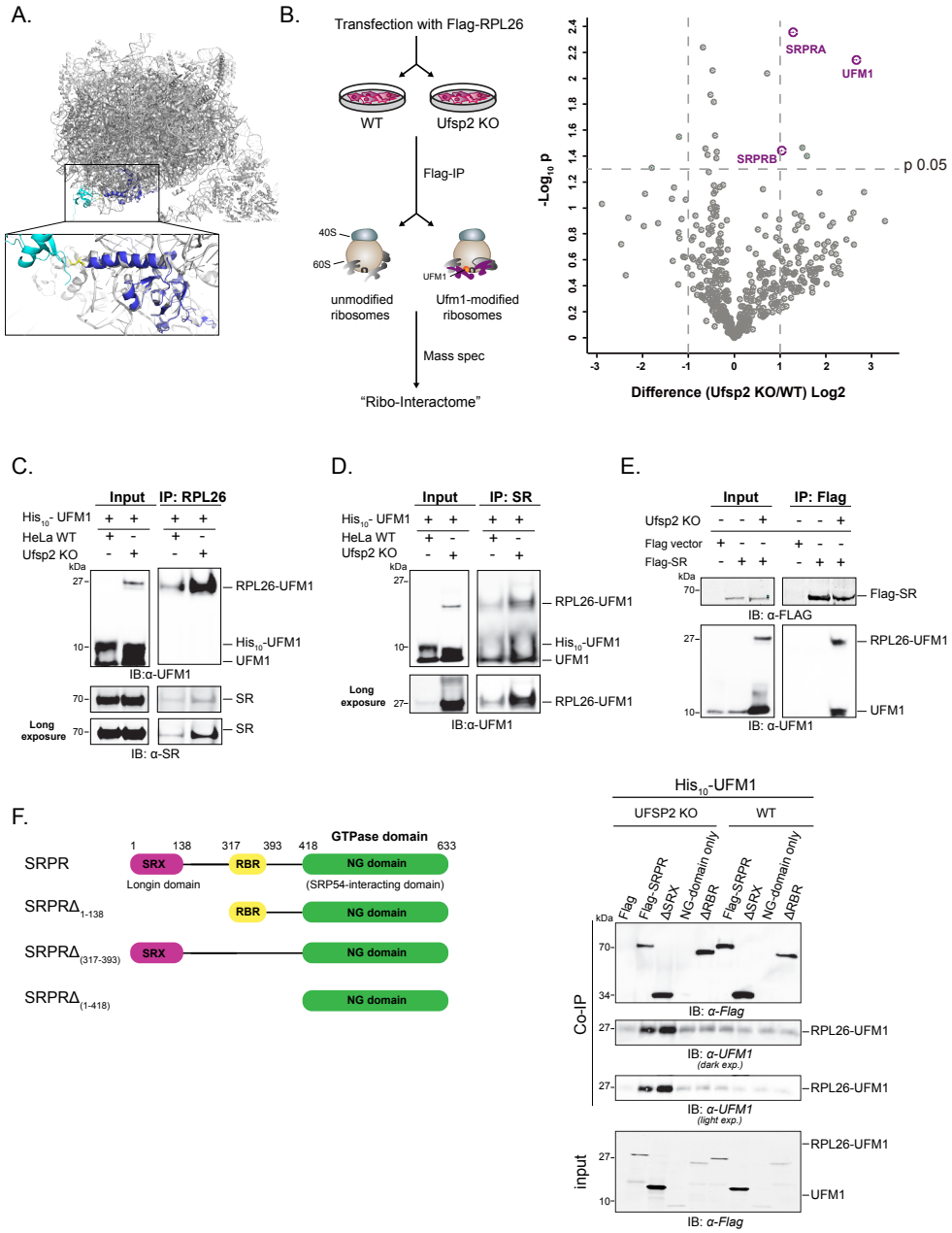

Figure 2 | A) Model indicating the position of UFM1-modified RPL26 relative to the SRP receptor as adapted from the structure of the human 80S ribosome (PDB 6FRK and 1WXS). B) Scheme illustrating the co-immunoprecipitation strategy utilized to identify RPL26-UFM1 interacting proteins. In the corresponding volcano plot, the predominant interactors (SRPRA (SRα), SRPRB (SRβ), and UFM1) are colored in magenta. C-D) Confirmation of the interaction of endogenous SRPRA (SRα) and RPL26-UFM1 by co-immunoprecipitation analysis.

Figure 2 | ***continued.*** E) Overexpressed Flag-SRα co-immunoprecipitates with endogenous RPL26-UFM1. F) Schematic representation of the SRα-domain organization and construct design. Co-immunoprecipitation assays with these Flag-SRα domain constructs reveal that the RBR-domain mediates the interaction with UFMylated RPL26.

UFMylation perturbs translational dynamics

Interaction between the ribosome and the translocon stipulates that ribosomes are translationally active[40], and thus we assessed the translational activity of UFMylated ribosomes by incubating either wild type, UFM1-, or UFSP2-depleted HeLa cells with 200 nM puromycin for 10 minutes subsequent to anti-puromycin antibody detection (Figure 3A and B). Unexpectedly, UFM1 depletion not only seems to increase translational activity compared to the wild type HeLa cells, but leads to an accumulation of puromycin labeled proteins with a lower molecular weight (Figure 3A). By contrast, UFSP2 depletion elicits an increased sensitivity towards puromycin at low concentrations (5 µg) while stable overexpression of His_{10}-UFM1 in both wild type and UFSP2-depleted HeLa cells decreased overall translation activity (Figure 3C). The observations that UFM1 depletion or the perturbation of its dynamics (i.e. UFSP2 depletion) underscore the participation of UFMylation in protein translation. Given the marked difference of ribosomal translation activity upon perturbation of UFMylation (Figure 3A-C), we have undertaken ribosome profiling experiments to pinpoint which proteins are altered. However, ribosome profiling of both wild type and UFSP2-depleted HeLa cells stably expressing His_{10}-UFM1 revealed no sftriking differences in mRNA translation (Figure S3E). Taking the puromycinylation assays into account (Figure 3A-C), the ribosome profiling experiments suggest that UFMylation might predominantly impact newly synthesized proteins rather than mRNA translation dynamics.

Furthermore, we investigated translational inhibitors with different mode of action induce ribosomal UFMylation by treating HeLa cells either with anisomycin, a peptidyl-transfer inhibitor[41, 42], or with cycloheximide, an translation elongation inhibitor[43]. Surprisingly, inhibition with 200 nM anisomycin for 30 minutes already robustly induced RPL26 UFMylation on up to three lysine residues (Figure 3D and E) leading to the subsequent relocalization of these modified ribosomes to the ER membrane, as assessed by differential centrifugation (Figure 3E). However, prolonged incubation with anisomycin did not significantly increase the amount of UFMylation of RPL26 (Figure 3D-F). By contrast, cycloheximide had a less pronounced effect upon ribosomal UFMylation, requiring 60 minutes to induce UFMylation (Figure S3A), which is reversed upon inhibitor washout (Figure S3C and 3D). Inspired by the observation that translational inhibitors induce UFMylation, we proceeded to explore whether inhibition with either anisomycin or cycloheximide would promote the interaction of UFMylated RPL26 with SRα. However, despite inducing UFMylation of RPL26 upon inhibitor treatment, the affinity between Flag-SRα and UFMylated RPL26 in either wild type or UFSP2-depleted HeLa cells could not be detected.

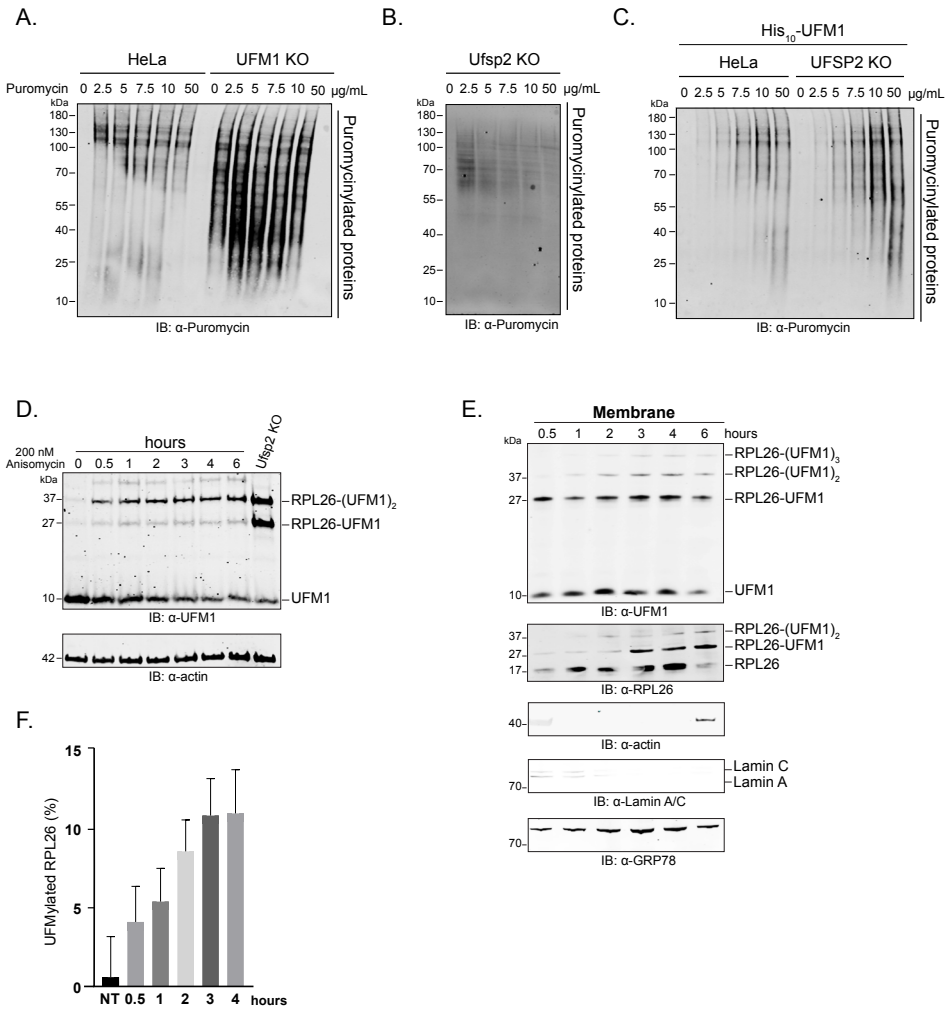

Figure 3 | UFMylation alters ribosomal translation dynamics. A-B) Treatment of wild type, UFM-1, or UFSP2-depleted HeLa cells or C) wild-type or UFSP2 deficient His_{10}-UFM1 expressing Hela cells with puromycin and subsequent analysis by immunoblotting with an anti-puromycin antibody. D) Incubation of HeLa cells with 200 nM anisomycin for the indicated time prior to immunoblotting of whole cell extracts against UFM1. E) Membrane enrichment after anisomycin treatment and subsequent visualization of UFMylated RPL26 using UFM1 and RPL26 antibodies, respectively. F) Corresponding quantification of the band intensity (error bars, SD, n= 3) expressed as percentage of UFMylated ribosomes localizing to the membrane after anisomycin treatment as shown in E).

In the light of our experimental data, evidence that UFM1-modified RPL26 increases the affinity of the ribosome towards SRα, but also observe that perturbation of UFMylation modulates ribosomal translational activity is provided. Moreover, our study demonstrates

that ribosomal stalling induced by translational inhibitors such as anisomycin or cycloheximide[44] stimulates UFMylation. From the experimental evidence, we conclude that ribosomal UFMylation might serve two functions: Firstly, promoting the interaction between the ribosome and SRα, and secondly to regulate translational rate of the ribosome perhaps to allow interaction of the emerging signal sequence with the SRP and the SRP receptor.

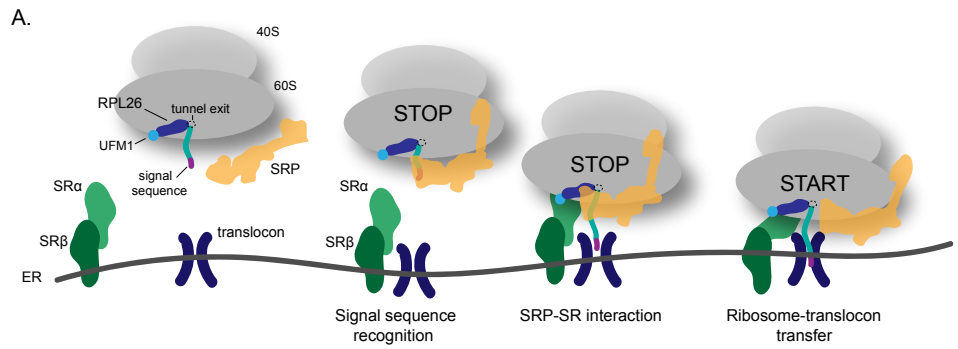

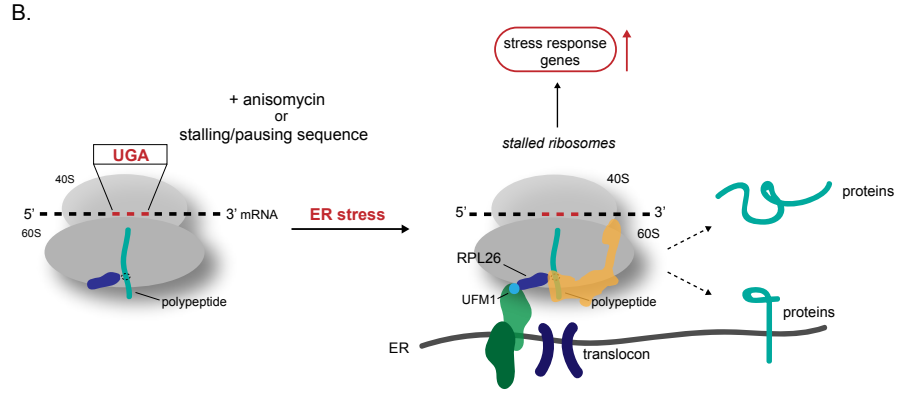

Figure 4 | Model depicting possible roles for RPL26 UFMylation. A) Upon UFMylation of RPL26, the affinity of the ribosome for SRα increases markedly, while perhaps stabilizing weakly hydrophobic signal sequences to facilitate the opening of the SEC61 channel gate. Additionally, ribosomal UFMylation might also stabilize certain conformations of the ribosome during handover of the nascent protein into the translocon. B) Upon ribosomal stalling induced by inhibitors (e.g. anisomycin) or by translational pausing (e.g. stop codon read-through), ER stress with concurrent ribosomal UFMylation and upregulation of stress response genes is elicited. UFMylated ribosomes localize to the ER membrane, possibly as a means to ensure proper localization of the translated protein.

Discussion

The accumulating evidence that UFM1 modification is crucial in a variety of fundamental biological process such as embryogenesis, blood progenitor development, and protein translation, necessitates the systematic identification of its substrates. To address this unmet need, we utilized a proteomics methodology that permitted us to identify the UFM1-modified substrate proteins and to pinpoint the acceptor lysines. Although our data indicates that the ribosomal protein RPL26 is the most abundant UFM1 substrate in response to UFSP2 depletion, five other potential UFMylation substrates, still awaiting validation due to technical difficulties, were uncovered. Unexpectedly, UFMylated RPL26 was found to associate with the SRP receptor (SRα) through virtue of its ribosome binding domain thus connecting UFMylation with the SRP-protein translocation pathway. Although the interaction of UFMylated RPL26 with the SEC61/62 translocon[7] has been reported, our data clearly indicates that this is an unlikely event. Firstly, it has been well established that only translating ribosomes associate with the translocon[40], and secondly binding of the UFMylated ribosome to the SRα temporally precedes the downstream interaction with the translocon. Furthermore, we provide evidence that the translation rates of nascent proteins rather than the mRNA translation rates are altered upon perturbation of UFMylation dynamics.

Taking the observations of previous reports of RPL26-UFMylation[7, 45] into account, we propose two models that integrate our data. From a structural perspective, RPL26-UFMylation, increases the SR-ribosome affinity, perhaps as a means to stabilize certain conformations during the RNC transfer to the translocon. Given that the ribosome-SR interaction accelerates the RNC transfer to the translocon[36], UFMylation of RPL26 increases the affinity for SRα with a concurrent decrease of nascent protein translation rates, introducing fidelity to RNC membrane targeting. Recently, the significance of SRα for the transfer of the ribosome nascent chain to the Sec61 channel has been reported[46]. Subsequent to SEC61 priming through ribosome binding, the emerging signal sequence opens both the lateral and the luminal gates of the channel for insertion into the ER membrane[47]. Especially proteins containing a weak hydrophobic signal sequence, such as the prion protein[46, 48], reside longer in the cytosol as gate opening is slowed, resulting in a decreased affinity of the ribosome for the translocon[40, 46, 49-51]. Thus, stabilization of the SRα-ribosome-RNC complex through ribosomal UFMylation would represent a unique mechanism to increase the SR-ribosome on-rate thereby permitting opening of the Sec61 channel by weakly hydrophobic signal sequence peptides[51, 52] while simultaneously decreasing the RNC-translation rate (Figure 4A).

Because of the participation of the SRP pathway, it is tempting to speculate that UFMylation of RPL26 affects only protein translocation into the ER membrane through association with

the Sec61 channel. Given that translational arrest induced by inhibitors induces UFMylation of RPL26, it is conceivable that UFM1 modification of the ribosome and subsequent engagement of the SRα receptor might facilitate the proper localization of proteins encoded by mRNA sequences causing ribosome stalling or prolonged pausing (Figure 4B).

However, induction of translational arrest by inhibitors such as anisomycin result in aberrant translation products that misfold or aggregate[53]. To facilitate the clearance of these defective proteins at the ER membrane, a specialized quality control pathway needs to be activated. In this context, the UFM1 system might contribute to the effective proteasomal or lysosomal processing of aberrant translation products[45].

Yet, these observations warrant further investigation to understand what proteins require the interaction between RPL26-UFM1 and SRα for efficient ER targeting. Furthermore, structural studies to visualize the conformational changes occurring upon SRα recruitment in the presence of a UFM1-modified ribosome would shed light into the complex mechanisms underlying SRP-mediated protein translocation.
Collectively, the data presented here demonstrate that UFM1-modification of RPL26 mediates the interaction of the ribosome with SRα increasing its on-rate, perhaps in order to allocate sufficient time for channel opening by proteins with weak hydrophobic signal sequences. Additionally, we report that ribosomal UFMylation decreases the nascent protein translation rate significantly, while absence of UFM1 leads to its acceleration. In the light of the increased affinity of the ribosome for SRα upon RPL26 UFMylation, we hypothesize that this translational slowdown represents a mechanism to provide fidelity to SRP-mediated protein targeting. Nonetheless, further research to elucidate the impact of this novel pathway in the context of cellular homeostasis and which proteins require this UFM1-mediated quality control mechanism needs to be undertaken.

While the complete extent of this intriguing alternative quality control mechanism awaits further dissection, the discovery that UFM1 mediates the affinity between SRα and the ribosome to promote targeting fidelity while simultaneously modulating translation rates of the nascent proteins suggests a unique and pivotal physiological role of the UFM1 system.

References

1. Cai, Y., N. Singh, and H. Li, Essential role of Ufm1 conjugation in the hematopoietic system. Exp Hematol, 2016. 44(6): p. 442-6.
2. Cai, Y., et al., UFBP1, a Key Component of the Ufm1 Conjugation System, Is Essential for Ufmylation-Mediated Regulation of Erythroid Development. PLoS Genet, 2015. 11(11): p. e1005643.
3. Hu, X., et al., Ubiquitin-fold modifier 1 inhibits apoptosis by suppressing the endoplasmic reticulum stress response in Raw264.7 cells. Int J Mol Med, 2014. 33(6): p. 1539-46.
4. Liu, J., et al., A critical role of DDRGK1 in endoplasmic reticulum homoeostasis via regulation of IRE1alpha stability. Nat Commun, 2017. 8: p. 14186.
5. Zhang, Y., et al., Transcriptional regulation of the Ufm1 conjugation system in response to disturbance of the endoplasmic reticulum homeostasis and inhibition of vesicle trafficking. PLoS One, 2012. 7(11): p. e48587.
6. Azfer, A., et al., Activation of endoplasmic reticulum stress response during the development of ischemic heart disease. Am J Physiol Heart Circ Physiol, 2006. 291(3): p. H1411-20.
7. Walczak, C.P., et al., Ribosomal protein RPL26 is the principal target of UFMylation. Proc Natl Acad Sci U S A, 2019.
8. Simsek, D., et al., The Mammalian Ribo-interactome Reveals Ribosome Functional Diversity and Heterogeneity. Cell, 2017. 169(6): p. 1051-1065 e18.
9. Zhu, H., et al., Ufbp1 promotes plasma cell development and ER expansion by modulating distinct branches of UPR. Nat Commun, 2019. 10(1): p. 1084.
10. Yoo, H.M., et al., Modification of ASC1 by UFM1 is crucial for ERalpha transactivation and breast cancer development. Mol Cell, 2014. 56(2): p. 261-274.
11. Li, J., et al., Ufm1-Specific Ligase Ufl1 Regulates Endoplasmic Reticulum Homeostasis and Protects Against Heart Failure. Circ Heart Fail, 2018. 11(10): p. e004917.
12. Yang, R., et al., CDK5RAP3, a UFL1 substrate adaptor, is critical for liver development. Development, 2019.
13. Zhang, M., et al., RCAD/Ufl1, a Ufm1 E3 ligase, is essential for hematopoietic stem cell function and murine hematopoiesis. Cell Death Differ, 2015. 22(12): p. 1922-34.
14. Low, K.J., et al., Hemizygous UBA5 missense mutation unmasks recessive disorder in a patient with infantile-onset encephalopathy, acquired microcephaly, small cerebellum, movement disorder and severe neurodevelopmental delay. Eur J Med Genet, 2018.
15. Mignon-Ravix, C., et al., Abnormal function of the UBA5 protein in a case of early developmental and epileptic encephalopathy with suppression-burst. Hum Mutat, 2018. 39(7): p. 934-938.
16. Arnadottir, G.A., et al., Compound heterozygous mutations in UBA5 causing early-onset epileptic encephalopathy in two sisters. BMC Med Genet, 2017. 18(1): p. 103.
17. Colin, E., et al., Biallelic Variants in UBA5 Reveal that Disruption of the UFM1 Cascade Can Result in Early-Onset Encephalopathy. Am J Hum Genet, 2016. 99(3): p. 695-703.
18. Lu, H., et al., The identification of potential factors associated with the development of type 2 diabetes: a quantitative proteomics approach. Mol Cell Proteomics, 2008. 7(8): p. 1434-51.
19. Tatsumi, K., et al., A novel type of E3 ligase for the Ufm1 conjugation system. J Biol Chem, 2010. 285(8): p. 5417-27.
20. Kang, S.H., et al., Two novel Ubiquitin-fold modifier 1 (Ufm1)-specific proteases, UfSP1 and UfSP2. J Biol Chem, 2007. 282(8): p. 5256-62.
21. Fulzele, A. and E.J. Bennett, Ubiquitin diGLY Proteomics as an Approach to Identify and Quantify the Ubiquitin-Modified Proteome. Methods Mol Biol, 2018. 1844: p. 363-384.
22. Pirone, L., et al., A comprehensive platform for the analysis of Ubiquitin-like protein modifications using in vivo biotinylation. Sci Rep, 2017. 7: p. 40756.
23. Hendriks, I.A. and A.C. Vertegaal, A high-yield double-purification proteomics strategy for the identification of SUMO sites. Nat Protoc, 2016. 11(9): p. 1630-49.
24. Simsek, D. and M. Barna, An emerging role for the ribosome as a nexus for post-translational modifications. Curr Opin Cell Biol, 2017. 45: p. 92-101.
25. Juszkiewicz, S. and R.S. Hegde, Initiation of Quality Control during Poly(A) Translation Requires Site-Specific Ribosome Ubiquitination. Molecular Cell, 2017. 65(4): p. 743-+.
26. Matsuo, Y., et al., Ubiquitination of stalled ribosome triggers ribosome-associated quality control. Nature Communications, 2017. 8.
27. El Motiam, A., et al., Interplay between SUMOylation and NEDDylation regulates RPL11 localization and function. FASEB J, 2019. 33(1): p. 643-651.
28. Schibich, D., et al., Global profiling of SRP interaction with nascent polypeptides. Nature, 2016. 536(7615): p. 219-23.
29. Walter, P., I. Ibrahimi, and G. Blobel, Translocation of proteins across the endoplasmic reticulum. I. Signal recognition protein (SRP) binds to in-vitro-assembled polysomes synthesizing secretory protein. J Cell Biol, 1981. 91(2 Pt 1): p. 545-50.
30. Tajima, S., et al., The signal recognition particle receptor is a complex that contains two distinct polypeptide chains. J Cell Biol, 1986. 103(4): p. 1167-78.
31. Wild, K., et al., Reconstitution of the human SRP system and quantitative and systematic analysis of its ribosome interactions.Nucleic Acids Res, 2019. 47(6): p. 3184-3196.
32. Wild, K., et al., SRP meets the ribosome. Nat Struct Mol Biol, 2004. 11(11): p. 1049-53.
33. Voorhees, R.M. and R.S. Hegde, Structures of the scanning and engaged states of the mammalian SRP-ribosome complex. Elife, 2015. 4.
34. Jadhav, B., et al., Mammalian SRP receptor switches the Sec61 translocase from Sec62 to SRP-dependent translocation. Nat Commun, 2015. 6: p. 10133.
35. Ogg, S.C., W.P. Barz, and P. Walter, A functional GTPase domain, but not its transmembrane domain, is required for function of the SRP receptor beta-subunit. J Cell Biol, 1998. 142(2): p. 341-54.
36. Mandon, E.C., Y. Jiang, and R. Gilmore, Dual recognition of the ribosome and the signal recognition particle by the SRP receptor during protein targeting to the endoplasmic reticulum. J Cell Biol, 2003. 162(4): p. 575-85.
37. Jiang, Y., et al., An interaction between the SRP receptor and the translocon is critical during cotranslational protein translocation. J Cell Biol, 2008. 180(6): p. 1149-61.
38. Pool, M.R., et al., Distinct modes of signal recognition particle interaction with the ribosome. Science, 2002. 297(5585): p. 1345-8.
39. Voorhees, R.M., et al., Structure of the mammalian ribosome-Sec61 complex to 3.4 A resolution. Cell, 2014. 157(7): p. 1632-43.

40. Conti, B.J., et al., Cotranslational stabilization of Sec62/63 within the ER Sec61 translocon is controlled by distinct substrate-driven translocation events. Mol Cell, 2015. 58(2): p. 269-83.
41. Grollman, A.P., Inhibitors of protein biosynthesis. II. Mode of action of aniso-mycin. J Biol Chem, 1967. 242(13): p. 3226-33.
42. Grollman, A.P., Structural basis for the inhibition of protein biosynthesis: mode of action of tubulosine. Science, 1967. 157(3784): p. 84-5.
43. Schneider-Poetsch, T., et al., Inhibition of eukaryotic translation elongation by cycloheximide and lactimidomycin. Nat Chem Biol, 2010. 6(3): p. 209-217.
44. Simms, C.L., L.L. Yan, and H.S. Zaher, Ribosome Collision Is Critical for Quality Control during No-Go Decay. Mol Cell, 2017. 68(2): p. 361-373 e5.
45. Wang, L., et al., UFMylation of RPL26 links translocation-associated quality control to endoplasmic reticulum protein homeostasis. Cell Res, 2019.
46. Ziska, A., et al., The signal peptide plus a cluster of positive charges in prion protein dictate chaperone-mediated Sec61 channel gating. Biol Open, 2019. 8(3).
47. Voorhees, R.M. and R.S. Hegde, Structure of the Sec61 channel opened by a signal sequence. Science, 2016. 351(6268): p. 88-91.
48. Kim, S.J. and R.S. Hegde, Cotranslational partitioning of nascent prion protein into multiple populations at the translocation channel. Mol Biol Cell, 2002. 13(11): p. 3775-86.
49. Rane, N.S., et al., Signal sequence insufficiency contributes to neurodegeneration caused by transmembrane prion protein. J Cell Biol, 2010. 188(4): p. 515-26.
50. Noriega, T.R., et al., Signal recognition particle-ribosome binding is sensitive to nascent chain length. J Biol Chem, 2014. 289(28): p. 19294-305.
51. Dudek, J., et al., Protein transport into the human endoplasmic reticulum. J Mol Biol, 2015. 427(6 Pt A): p. 1159-75.
52. Pfeffer, S., et al., Structure of the mammalian oligosaccharyl-transferase complex in the native ER protein translocon. Nat Commun, 2014. 5: p. 3072.
53. Stein, K.C. and J. Frydman, The stop-and-go traffic regulating protein biogenesis: How translation kinetics controls proteostasis. J Biol Chem, 2019. 294(6): p. 2076-2084.

Supplementary Information

Material and Methods

Cloning

To generate the His_{10}-Ufm1_K0 construct used in this study, the nucleotides corresponding to the following amino acid sequence were subcloned into the lentiviral pLV-CMV-IRES-puro vector[1]: MHHHHHHHHHHGGSMSRVSFRITLTSDPRLPYRVLSVPESTPFTAVLRFAAEEFRVPAATSAIITNDGIGINPAQTGNVFLRHGSELRIIPRDRVG. RPL26 was subcloned from a Gateway pDONR 223 vector into a pCSF107mT Gateway vector (Addgene, plasmid # 67619) containing an C-terminal Flag epitope-tag. Mutagenesis of the identified lysines 132-136 to arginine in Flag-RPL26 was performed according to the protocol of the Quik Change Site-directed Mutagenesis Kit (Invitrogen). SRPRA (SRα) was amplified from cDNA and cloned into a Flag-C1 vector (Clontech) using BglII/BamHI restriction sites. The SRα domain constructs were generated from Flag-SRα with appropriate primers by IVA cloning[2] . All constructs were verified by sequencing.

Cell culture and cell line generation

The HeLa cell line originated from the ATCC and were cultured under standard conditions in Dulbecco's modified Eagle's medium (Gibco Invitrogen Corporation, Grand Island, NY, USA) supplemented with 10% FBS (Gibco) at 37°C with 5% CO2. All cell lines were routinely tested for mycoplasma contamination with consistently negative outcomes. Hela cells (60% confluency) were infected using a bicistronic lentivirus encoding His10_UFM1_K0_IRES_puro at a MOI of 3 and grown for two weeks under puromycin selection (2.5 µM) and subsequently validated by immunoblotting using antibodies against the His-tag and UFM1.

CRISPR-CAS mediated gene editing

Guide RNAs (gRNA) for UFSP2 and UFM1 were designed using the CRISPR Design tool (http://crispr.mit.edu/), and subcloned into a pX330-U6-Chimeric_BB-CBh-hSpCas9 vector (Addgene, plasmid # 42230, Cambridge, MA, USA), a human codon-optimized SpCas9 and chimeric guide RNA expression plasmid[3]. CRISPR-mediated UFSP2 and UFM1 depletion was achieved by co-transfecting confluent HeLa cells with the vector harboring the gRNA and the Cas9 together with a construct conferring the blasticidin resistance[4]. Following blasticidin selection and clonal expansion, USFP2 and UFM1 depletion were verified by immunoblotting with antibodies against UFSP2 and UFM1.

Electrophoresis and immunoblotting

Whole cell extracts or purified protein samples were separated on Novex Bolt 4-12% Bis-Tris Plus gradient gels (Life Technologies) using MOPS buffer or via regular SDS-PAGE using a

Tris-glycine buffer and transferred onto Hybond-C nitrocellulose membranes (GE Healthcare Life Sciences). Membranes were stained with Ponceau S (Sigma) to stain total protein and blocked with PBS containing 5% milk powder before incubating with the primary and secondary antibodies as indicated.

Antibodies

For visualization western blotting was performed as previously described and membranes probed with rabbit Ufsp2 antibody (1:1000 dilution; Abcam ab192597), rabbit Ufm1 antibody (1:1000 dilution; Abcam ab109305), rabbit RPL26 antibody (1:1000 dilution; Sigma PA5-17093 and Abcam ab59567), rabbit SRPR antibody (1:1000 dilution, ab228625), mouse Flag-M2 antibody (1:1000 dilution; Sigma F1804), mouse anti-Puromycin antibody clone 12D10 (Merck-Millipore, MABE343), rabbit anti-Lamin A/C (Santa Cruz, sc-376248), rabbit anti-GRP78 (Abcam, ab108615), and mouse anti-β-actin antibody (1:10000 dilution; Sigma A5541). Fluorescent secondary antibodies anti-mouse-800 (1:1000 dilution; LiCOR 926-3210) and anti-rabbit-800 (1:10000 dilution; LiCOR, 926-3211) were used for visualization of labeled proteins on LiCOR Odyssey system 3.0. Alternatively, membranes were probed with HRP-Protein A secondary antibody (1:5000 dilution, Thermo Fisher, 101023) prior to incubation with SUPER Signal West Dura Extended Duration Signal Substrate (ECL, Thermo Fisher), with subsequent visualization using the Amersham Imager AI600.

Immunoprecipitation

To identify interacting proteins, co-immunoprecipitation was performed by scraping cells on ice into Co-IP buffer (50mM Tris-HCl, pH 7.5, 1.5mM MgCl2, 5% Glycerol, 0,5% NP-40 and Complete Protease Inhibitor tablet (Roche)), briefly sonicating the samples on ice, and clarifying them by centrifugation (max speed, 4°C, 20 min) to remove cell debris. Cell lysates were then incubated with 30 µL Protein-G agarose and 2 µg mouse Flag-M2 antibody (Sigma, F1804), rabbit RPL26 antibody (Sigma PA5-17093), or rabbit SRPR antibody (ab228625) overnight at 4°C while rotating. Following incubation, beads were pelleted (500 rpm, 4°C, 5 min), supernatant removed and four washes with ice-cold Co-IP buffer performed, with transfer of the sample to fresh microcentrifuge tubes before the last wash. Samples were then further processed for mass spectrometry by on-bead trypsin digestion, as further described. For the immunoblots, 35 µL 3x SDS-PAGE loading buffer was added to the samples followed by boiling at 95°C for 10 minutes and resolution on a 4-12% SDS-PAGE gel (NuPAGE, Invitrogen). After transfer to nitrocellulose, membranes were probed with rabbit UFM1 antibody, rabbit RPL26 antibody, and mouse SRPR alpha antibody and secondary rabbit anti-mouse Immunoglobulin-HRP (1:10000 dilution; Dako) and HRP-Protein A (1:10000 dilution; Invitrogen 10123) antibodies. Proteins were visualized using Super Signal West Dura Extended Duration Signal Substrate ECL (Thermofisher, 34075) on an Amersham imager AI600.

Puromycinylation and translation inhibition assays

To assay translational activity, confluent wildtype, UFM or UFSP2-depleted HeLa cells or His_{10}-UFM1K0 expressing cell lines were incubated with 2.5-50 µg/mL puromycin for 10 minutes prior to lysis and subsequent immunoblotting. For the translation inhibitor treatments, cells were incubated with either 50 µg/mL cycloheximide (Sigma Aldrich, C7698) or 200 nM anisomycin (Sigma Aldrich, A9789) for the indicated time. Inhibitor washout experiments were performed by incubating the cells for the indicated time with either cycloheximide or anisomycin, removing the inhibitor containing media, washing with PBS and incubating the cells in DMEM supplemented with 10% FCS for the indicated time prior to further processing for immunoblot analysis.

Purification of His_{10}-UFM1 conjugates

Hela cells expressing His_{10}-UFM1-K0 were washed, scraped and collected in ice-cold PBS. For total lysates, a small aliquot of cells was kept separately and lysed in 2% SDS, 1% N-P40, 50 mM TRIS pH 7.5, 150 mM NaCl. The remaining part of the cell pellets were lysed in 6 M guanidine-HCl pH 8.0 (6 M guanidine-HCl, 0.1 M Na_2HPO_4/NaH_2PO_4, 10 mM TRIS, pH 8.0). The samples were snap frozen using liquid nitrogen, and stored at -80°C.

For His_{10}-UFM1-K0 purification, the cell lysates were first thawed at room temperature and sonicated for 5 sec using a sonicator (Misonix Sonicator 3000) at 30 Watts to homogenize the lysate. Protein concentrations were determined using the bicinchoninic acid (BCA) protein assay reagent (Thermo Scientific) and lysates were equalized. Subsequently, imidazole was added to a final concentration of 50 mM and β-mercaptoethanol was added to a final concentration of 5 mM. His10-UFM1-K0 conjugates were enriched on nickel-nitrilotriacetic acid-agarose beads (Ni-NTA) (Qiagen), and subsequently the beads were washed using wash buffers A-D. Wash buffer A: 6 M guanidine-HCl, 0.1 M Na_2HPO_4/NaH_2PO_4 pH 8.0, 0.01 M Tris-HCl pH 8.0, 10 mM imidazole pH 8.0, 5 mM β-mercaptoethanol, 0.1% Triton X-100. Wash buffer B: 8 M urea, 0.1 M Na_2HPO_4/NaH_2PO_4 pH 8.0, 0.01 M Tris-HCl pH 8.0, 10 mM imidazole pH 8.0, 5 mM β-mercaptoethanol, 0.1% Triton X-100. Wash buffer C: 8 M urea, 0.1 M Na_2HPO_4/NaH_2PO_4 pH 6.3, 0.01 M Tris-HCl pH 6.3, 10 mM imidazole pH 7.0, 5 mM β-mercaptoethanol, no Triton X-100. Wash buffer D: 8 M urea, 0.1 M Na_2HPO_4/NaH_2PO_4 pH 6.3, 0.01 M Tris-HCl, pH 6.3, no imidazole, 5 mM β-mercaptoethanol, no Triton X-100. Wash buffers employed for immunoblotting experiments contained 0.2% Triton X-100. Samples were eluted in 7 M urea, 0.1 M NaH_2PO_4/Na_2HPO_4, 0.01 M Tris/HCl, pH 7.0, 500 mM imidazole pH 7.0 and processed according to the method described by Hendriks *et al.*[5].

Sample preparation and mass spectrometry

UFM1-enriched samples were supplemented with 1M Tris-(2-carboxyethyl)-phosphine hydrochloride (TCEP) to a final concentration of 5 mM and incubated for 20 minutes at room temperature. Iodoacetamide (IAA) was then added to the samples to a 10 mM final concen-

tration, and samples were incubated in the dark for 15 minutes at room temperature. Lys-C and Trypsin digestions were performed according to the manufacturer's specifications. Lys-C was added in a 1:50 enzyme-to-protein ratio, samples were incubated at 37 °C for 4 hours, and subsequently 3 volumes of 100 mM Tris-HCl pH 8.5 were added to dilute urea to 2 M. Trypsin (V5111, Promega) was added in a 1:50 enzyme-to-protein ratio and samples were incubated overnight at 37 °C. For site-specific samples preparation, we used the strategy developed previously by our group[5].

Subsequently, digested samples were desalted and concentrated on STAGE-tips as described previously (40) and eluted with 80% acetonitrile in 0.1% formic acid. Eluted fractions were vacuum dried employing a SpeedVac RC10.10 (Jouan, France) and dissolved in 10 µL 0.1% formic acid before online nanoflow liquid chromatography-tandem mass spectrometry (nanoLC-MS/MS). All the experiments were performed on an EASY-nLC 1000 system (Proxeon, Odense, Denmark) connected to a Q-Exactive Orbitrap or a Q-Exactive Plus Orbitrap (Thermo Fisher Scientific, Germany) through a nano-electrospray ion source. For the Q-Exactive, peptides were separated in a 13 cm analytical column with an inner-diameter of 75 µm, in-house packed with 1.8 µm C18 beads (Reprospher-DE, Pur, Dr. Manish, Ammerbuch-Entringen, Germany). The Q-Exactive Plus was coupled to 15 cm analytical columns with an inner-diameter of 75 µm, in-house packed with 1.9 µm C18 beads (Reprospher-DE, Pur, Dr. Manish, Ammerbuch-Entringen, Germany), employing a column oven (PRSO-V1, Sonation, Biberach) to heat the column to 50 °C.

The gradient length was 120 minutes from 2% to 95% acetonitrile in 0.1% formic acid at a flow rate of 200 nL/minute. The mass spectrometers were operated in data-dependent acquisition mode with a top 10 method. Full-scan MS spectra were acquired at a target value of 3 x 106 and a resolution of 70,000, and the Higher-Collisional Dissociation (HCD) tandem mass spectra (MS/MS) were recorded at a target value of 1 x 105 and with a resolution of 17,500 with a normalized collision energy (NCE) of 25%. The maximum MS1 and MS2 injection times were 20 ms and 60 ms, respectively. The precursor ion masses of scanned ions were dynamically excluded (DE) from MS/MS analysis for 60 sec. Ions with charge 1, and greater than 6 were excluded from triggering MS2 events. For samples enriched for identification of UFM1 acceptor lysines, a 120 minute gradient was used for chromatography. Data dependent acquisition with a top 5 method was used. Maximum MS1 and MS2 injection times were 20 ms and 250 ms, respectively. Resolutions, normalized collision energy and automatic gain control target were set as mentioned previously. Dynamic exclusion was set to 20 sec.

Mass Spec data analysis

Site-level UFMylation data analysis

Site-specific purification was performed in three biological replicates, and all samples were measured in technical duplicates. All 18 RAW files were analyzed by MaxQuant (version 1.5.3.30). the first search was carried out with a mass accuracy of 20 ppm, while the main search used 64.5 ppm for precursor ions. Database searches were performed with trypsin/P specificity, allowing three missed cleavages. Carbamidomethylation of cysteine residues was considered as a fixed modification. Mass tolerance of MS/MS spectra was set to 20 ppm to search against an in silico digested UniProt reference proteome for Homo Sapiens (2017-30-01). Additionally, MS/MS data were searched against a list of 245 common mass spectrometry contaminants by Andromeda. Oxidation (M) and Acetyl (Protein N-term) were set as variable modifications. VG-modified lysine was introduced as a variable modification with a composition of C7H12N2O2 and a monoisotopic mass of 156.090 Da. Match between runs was used with 0.7 min match time window and 20 min alignment time window.

Interactors of UFMylated RPL26

Protein lists generated by MaxQuant were further analyzed by Perseus (Version 1.5.5.3). Proteins identified only by site and as a common contaminant were filtered out, and then all the LFQ intensities were log2 transformed. Different experiments were annotated in six groups, Hela-Flag, Hela-Flag-RPL26, Hela-His10-UFM1K0-Flag, Hela-His10-UFM1K0-Flag-RPl26, Hela (ΔUFSP2)-His10-UFM1K0-Flag, Hela (ΔUFSP2)-His10-UFM1K0-Flag-RPL26. Proteins identified in at least one condition and in at least three biological replicates were included for further analysis. For each individual experimental condition, missing values were included using the Perseus software by normally distributed values with a 1.8 downshift (log2). Final corrected p-values were filtered to be less than 0.05. Then, the average log2 ratios for Hela-His10-Ufm-K0-Flag-RPL26 vs. Hela-His10-Ufm-K0-Flag were calculated and p-values of each protein across all conditions calculated by t-tests. Proteins with average log2 ratios > 1 and corresponding p values < 0.05 were considered as UFMylated-RPL26 interactors. The interactors were visualized graphically by a volcano plot.

Subcellular fractionation

To separate the cytosolic, nuclear, and total membrane fractions, a 10 cm dish of either confluent HeLa or Hela UFSP2 knockout cells stably expressing His_{10}-UFM1 were washed twice with ice-cold wash buffer (250 mM sucrose) and scraped in 250 µL isolation medium (250 mM D-mannitol, 5mM HEPES pH 7.4, and 0.5 mM EGTA). Cells were lysed by passing 10 times through a 26-gauge needle. Nuclei were pelleted at 600x g for 10 min at 4°C. To pellet total membranes, post-nuclear supernatants were centrifuged at 100,000x g for 2 hours at 4°C. The post-membrane supernatant was collected as cytosolic fraction.

Ribosome Pelleting

To enrich for membrane-bound ribosomes, the membranes were isolated from confluent wildtype or UFSP2-depleted cells as described above, before laying the membrane or cytosolic fractions on top of 1M sucrose and centrifuged at 48.000 rpm for 2h at 4°C using a SW55-Ti rotor (Beckman). Following centrifugation, the sucrose cushion was carefully removed and the pellets washed once with ribosome buffer (50 mM HEPES, pH 7.6, 100 mM KOAc, 5mM Mg(OAc)2) before adding SDS-PAGE sample buffer and subsequently separated by electrophoresis prior to immunoblotting using standard procedures.

Ribosome profiling

$3.0x10^5$ HeLa cells were treated with cycloheximide (100 µg/ml) for 5 minutes, washed with ice-cold PBS (cycloheximide, 100 µg/ml), and lysed in buffer A (20 mM Tris-HCl, pH 7.8, 100 mM KCl, 10 mM $MgCl_2$, 1% Triton X-100, 2 mM DTT, 100 µg/ml cycloheximide, 1X complete protease inhibitor). Lysates were centrifuged at 5,000 rpm and the supernatant was treated with 2 U/µl of RNase I (Thermo Scientific) for 45 min at room temperature. Lysates were fractionated on a linear sucrose gradient (7% to 47%) using the SW-41Ti rotor at 36,000 rpm for 2 h. Fractions enriched in monosomes were pooled and treated with proteinase K (Roche, Mannheim, Germany) in a 1% SDS solution. Released RNA fragments were purified using Trizol reagent following the manufacturer's instructions. For libraries preparation, RNA was gel-purified on a denaturing 10% polyacrylamide urea (7 M) gel. A section corresponding to 18 to 33 nucleotides, the region where most of the ribosome-protected fragments are comprised, was excised, eluted and ethanol precipitated. The resulting fragments were 3′-dephosphorylated using T4 polynucleotide kinase (NEB) for 4h at 37°C in 2-(N-morpholino)ethanesulfonic acid (MES) buffer (100 mM MES-NaOH, pH 5.5, 10 mM $MgCl_2$, 10 mM β-mercaptoethanol, 300 mM NaCl). 3′ adaptor was added with T4 RNA ligase 1 (NEB) for 2.5 h at 37°C. Ligation products were 5′-phosphorylated with T4 polynucleotide kinase for 30 min at 37°C. 5′ adaptor was added with T4 RNA ligase 1 for 18 h at 22°C. rRNA was depleted using custom biotinylated probes. Libraries were PCR amplified for 15 cycles and the purified PCR products were sequenced in an Illumina's HiSeq-2500 platform.

References

1. Vellinga, J., et al., A system for efficient generation of adenovirus protein IX-producing helper cell lines. J Gene Med, 2006. 8(2): p. 147-54.
2. Garcia-Nafria, J., J.F. Watson, and I.H. Greger, IVA cloning: A single-tube universal cloning system exploiting bacterial In Vivo Assembly. Sci Rep, 2016. 6: p. 27459.
3. Cong, L., et al., Multiplex genome engineering using CRISPR/Cas systems. Science, 2013. 339(6121): p. 819-23.
4. Blomen, V.A., et al., Gene essentiality and synthetic lethality in haploid human cells. Science, 2015. 350(6264): p. 1092-6.
5. Hendriks, I.A. and A.C. Vertegaal, A high-yield double-purification proteomics strategy for the identification of SUMO sites. Nat Protoc, 2016. 11(9): p. 1630-49.

A.

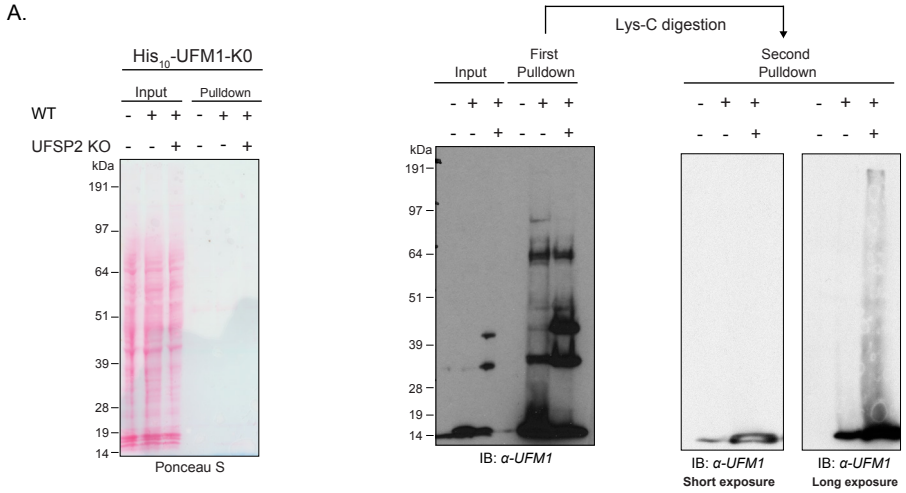

B.

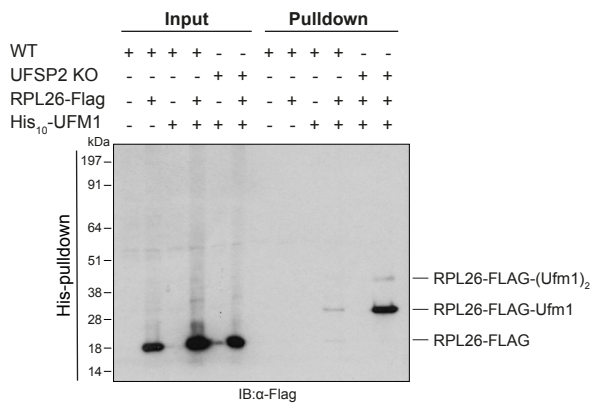

C.

Protein	UFM1-VG site	UFM1-VG site positions	Score
RPL26 / RPL26L1	132	KILERKAKSRQVGKE**K**GKYKEETIEKMQE__	210.35/140.14
RPL26 / RPL26L1	134	LERKAKSRQVGKEKG**K**YKEETIEKMQE____	100.22/62.16
RPL26 / RPL26L1	136	RKAKSRQVGKEKGKY**K**EETIEKMQE_____	69.03/60.16
RPL26	142	QVGKEKGKYKEETIE**K**MQE_____	64.84
TUBA1B	370	INYQPPTVVPGGDLA**K**VQRAVCMLSNTTAIA	92.93
MCM5	582	VRQLEAIVRIAEALS**K**MKLQPFATEADVEEA	61.16
SLC26A7	120	SIVVLVLVKELNEQF**K**RKIKVVLPVDLVLII	60.91
SCYL2	73	KQEVAVFVFDKKLID**K**YQKFEKDQIIDSLKR	59.91
SCYL2	76	VAVFVFDKKLIDKYQ**K**FEKDQIIDSLKR	59.91
WDR63	564	DHLLCKTQDKMLAQS**K**TEKAEEMNPYHNLES	45.28

Figure S1 | Denaturing His$_{10}$-UFM1 pulldown. A) Purification of His$_{10}$-UFM1-K0 conjugates under denaturing conditions (middle panel), followed by Lys-C digestion and a second purification on Ni-NTA-agarose (right panel). UFM1-modified proteins were visualized by

Figure S1 | *continued.* immunoblotting against UFM1 prior to analysis by mass spectrometry. Membranes were stained with Ponceau S prior to staining to verify equal loading (left panel). B) Validation that the three acceptor lysines (K132-K136) are indeed UFMylated by overexpression of Flag-RPL26 or the Flag-RPL26 (3KR) mutant followed by His-pulldown. Immunoblotting against the Flag-tagged RPL26, confirmed that these acceptor lysines are UFMylated. C) VG-sites identified for UFM-1 modified proteins identified by mass spectrometry.

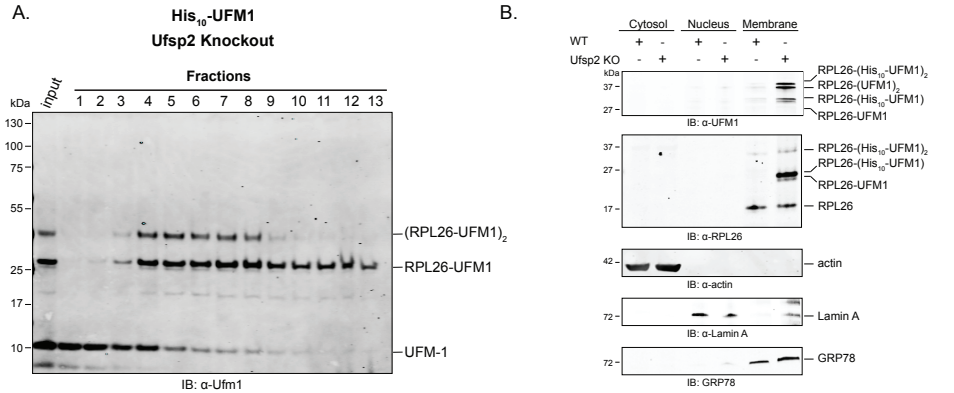

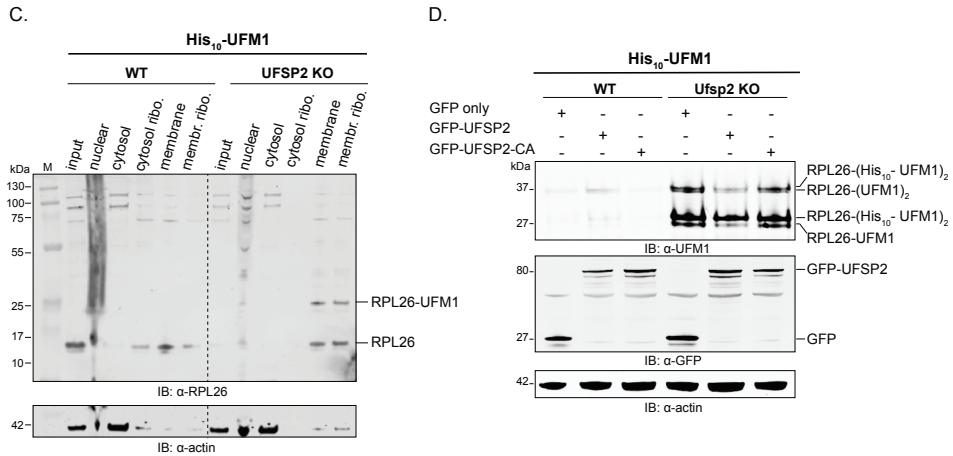

Figure S2 | UFMylated RPL26 is incorporated into membrane-bound 80S ribosomes. A) Ribosome purification using a 7-47% sucrose gradient and subsequent immunoblotting against UFM1 reveals that modified RPL26 is incorporated into the 80S ribosome. B) Membrane enrichment reveals that UFMylated RPL26 is targeted to membranes and C) subsequent ribosome pelleting confirms that only the membrane bound ribosomes are UFMylated. D) UFM1 modification of RPL26 in HeLa cells lacking UFSP2 can be reversed by transient transfection of GFP-UFSP2 but not by the catalytic inactive GFP-UFSP2_C302A mutant.

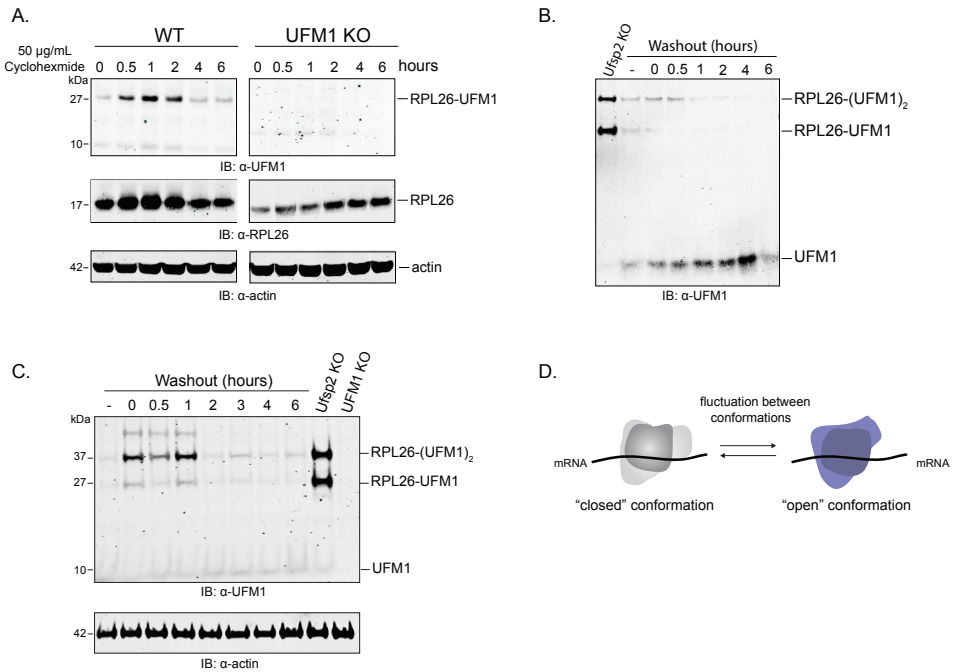

Figure S3 | Protein translation inhibitors induce ribosomal UFMylation. A) Incubation with 50 ug/mL cycloheximide for up to 6 hours induces RPL26-UFMylation and seems to promote RPL26 stability. B) Washout of cycloheximide following 1 hour incubation demonstrates the reversibility of RPL26 UFMylation after cycloheximide treatment. C) Washout of anisomycin after 30 minutes incubation results in gradual removal of UFM1 from RPL26. D) Scheme depicting the conformational changes of the ribosome upon treatment with cycloheximide (closed conformation) or anisomycin (open or rotated conformation). E) Metagene distribution of ribosome protected fragments (RPFs). Hela UFSP2 KO cells show a higher relative accumulation of ribosomes towards the 3' end of the coding sequence (CDS) and decreased ribosome density in the 5' end, suggesting either problems during the initial folding of the proteins or altered dynamics of the ribosome elongation.